Theoretical Examination of the S_N2 Reaction Involving Chloride Ion and Methyl Chloride in the Gas Phase and Aqueous Solution

Jayaraman Chandrasekhar,* Scott F. Smith, and William L. Jorgensen*

Contribution from the Department of Chemistry, Purdue University, West Lafayette, Indiana 47907. Received May 29, 1984

Abstract: The role of hydration on the course of the S_N2 reaction between chloride ion and methyl chloride has been studied by using quantum and statistical mechanical methods. The gas-phase reaction was examined at the ab initio molecular orbital level with the 6-31G* basis set. The calculated double-well potential surface is typical of gas-phase S_N2 profiles, featuring unsymmetrical ion–dipole complexes as minima and a symmetrical transition state. The complexation energy (10.3 kcal/mol) and intrinsic barrier (13.9 kcal/mol) compare favorably with experimental values. Monte Carlo simulations were then carried out for the solute cluster solvated by 250 water molecules at 25 °C and 1 atm by using solute–solvent potential functions derived from ab initio calculations in conjunction with the TIP4P model of water. In one set of simulations, importance sampling was employed to obtain the potential of the mean force in solution. The influence of the solvent is to make the reaction surface almost unimodal and to increase the barrier significantly. The calculated free energy of activation (26.3 kcal/mol) is in excellent agreement with the experimental estimate. Additional simulations were carried out in which the solute was held rigidly at geometries corresponding to the reactants/products and to the transition state. The solvation of the transition state relative to the separated species is characterized by less exothermic solute–solvent interaction as well as by a reduced solvent disruption energy. The increase in activation energy due to hydration is caused by reduction in strength rather than in the number of solute–solvent hydrogen bonds. The simulations provide detailed insights into the structural and energetic nature of the differential solvation of the reactants and transition state.

The rates of bimolecular nucleophilic substitution reactions involving anions and polar molecules vary over 20 orders of magnitude on going from the gas phase to polar, especially protic, media.[1-3] Even the qualitative nature of the reaction appears to be altered through solvation. The extensive studies of Brauman and co-workers have confirmed the double-well form of the potential surface for S_N2 reactions in the gas phase,[1,2] while in solution the energy profiles are generally believed to be unimodal.[3] The development of a detailed molecular level understanding of the role of solvation on the qualitative and quantitative nature of S_N2 reaction profiles has emerged as a fundamental goal in physical organic chemistry.

In his classic early work, Ingold noted that electrostatic solvation forces must be regarded as primary determinants of the activation energy for S_N2 reactions.[3a] He explained the observed rate differences on the basis of the charge distribution of the reactants and the transition state. For reactions involving anions and neutral substrates, one of the reactants has a localized charge while the transition state is characterized by a diffuse distribution. Application of Born's equation predicts a differential stabilization of the reactants by polar solvents, leading to increased activation barriers in such media. Later workers, especially Parker,[3c] emphasized the importance of specific solute–solvent interactions like hydrogen bonding as well as variation in solvent reorganization energies for the reactants and the transition state in highly structured solvents. Initial desolvation of the nucleophile before its approach to the substrate has also been proposed as a major contributor to the activation energy in protic solvents.[3e,f] Although these concepts have been of considerable interpretative value, largely empirical schemes have been adopted as predictive models.[3c,d,4,5] For example, a sound thermodynamic description of the role of solvents in some S_N2 reactions has been based on solvent activity coefficients, i.e., the change in the standard chemical potential of a solute on transfer from a reference solvent to another solvent for the reactants, transition states, and products.[3c] From a relatively small number of experimentally measurable quantities, a large body of rate data could be rationalized and often reduced to simple linear free-energy relationships. The Marcus equation has also been successfully applied to the prediction of S_N2 reactivity trends for nonidentity reactions in various solvents.[3d] Recently the Marcus theory has been employed in conjunction with valence bond state correlation diagrams to provide a unified description of S_N2 reactivities in the gas phase and in solution.[5]

Nevertheless, all the solution reaction models have been incomplete for at least one of the following reasons. (i) They are

(1) Review: Nibbering, N. M. M. In "Kinetics of Ion–Molecule Reactions"; Ausloos, P., Ed.; Plenum Press: New York, 1979.

(2) (a) Lieder, C. A.; Brauman, J. I. *J. Am. Chem. Soc.* **1974**, *96*, 4029. (b) Brauman, J. I.; Olmstead, W. N.; Lieder, C. A. *Ibid.* **1974**, *96*, 4030. (c) Olmstead, W. N.; Brauman, J. I. *Ibid.* **1977**, *99*, 4019. (d) Pellerite, M. J.; Brauman, J. I. *Ibid.* **1980**, *102*, 5993. For more gas-phase mechanistic work, see: Bohme, D. K.; Young, L. B. *J. Am. Chem. Soc.* **1970**, *92*, 7354. Bohme, D. K.; Mackay, G. I.; Payzant, J. D. *Ibid.* **1974**, *96*, 4027. Tanaka, K.; Mackay, G. I.; Payzant, J. D.; Bohme, D. K. *Can. J. Chem.* **1976**, *54*, 1643.

(3) (a) Ingold, C. K. "Structure and Mechanism in Organic Chemistry", 2nd ed.; Cornell University Press: Ithaca, NY, 1969. (b) Hartshorn, S. R. "Aliphatic Nucleophilic Substitution"; Cambridge University Press: London, 1973. (c) Parker, A. J. *Chem. Rev.* **1969**, *69*, 1. (d) Albery, W. J.; Kreevoy, M. M. *Adv. Phys. Org. Chem.* **1978**, *16*, 87. (e) Ritchie, C. D. In "Solute–Solvent Interactions"; Coetzee, J. F., Ritchie, C. D., Eds.; Marcel Dekker: New York, 1969; p 284. (f) Dewar, M. J. S.; Dougherty, R. C. "The PMO Theory of Organic Chemistry"; Plenum Press: New York, 1975; pp 234, 266. (g) Carrion, F.; Dewar, M. J. S. *J. Am. Chem. Soc.* **1984**, *106*, 3531.

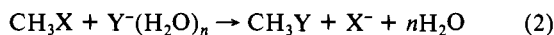(4) McLennan, D. J. *Aust. J. Chem.* **1978**, *31*, 1897.

(5) Shaik, S. S. *J. Am. Chem. Soc.* **1984**, *106*, 1227.

S_N2 Reaction of Chloride Ion and Methyl Chloride

J. Am. Chem. Soc., Vol. 107, No. 1, 1985 155

mostly qualitative in nature. (ii) The discussions focus on the energetics of only a few points on the reaction surface, namely, the reactants, transition states, and the products. Attempts are seldom made to provide a complete description of the potential energy surface. In particular, the unimodal nature of the solution reaction profile is implicitly assumed. (iii) The most serious limitation of these models is the lack of sufficient molecular detail in accounting for the differential solvation effect.

In contrast to condensed-phase reactions, considerable progress has been made in characterizing the energetics of S_N2 reactions in the gas phase through the application of quantum mechanical methods.[6,7] Ab initio calculations with large basis sets correctly reproduce the double-well-potential surface and provide valuable information concerning the geometries, charge distributions, and energies of points along the reaction coordinate. However, explicit inclusion of solvent effects is beyond the scope of current quantum mechanical methods. Recently, an interesting attempt along these lines has been made in which the reaction of methyl chloride with a chloride ion solvated by one and two water molecules was investigated.[8] The calculated barrier was found to be increased significantly with the introduction of only one or two solvent molecules. The model system was considered to be bridge linking gas-phase and solution-phase reactions. Although these results are intrinsically interesting and have a direct bearing on gas-phase reactions of solvated clusters,[9,10] their relevance to a solution-phase reaction is debatable. The cluster reactions do not include the significant contribution of bulk solvent reorganization to the activation barrier in solution and the effects of statistical averaging. Even the qualitative nature of the cluster and solution-phase reactions may be different.[10] For the reaction in dilute solution, eq 1, the solutes are solvated as effectively as possible at all points along the reaction coordinate. Thus, the desolvation of the

$$CH_3X \text{ (aq)} + Y^- \text{ (aq)} \rightarrow CH_3Y \text{ (aq)} + X^- \text{ (aq)} \qquad (1)$$
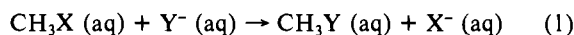
nucleophile and the solvation of the leaving group occur synchronously about the transition state due to the presence and participation of bulk solvent molecules. Cluster models may not adequately represent these processes due to ineffective transfer of solvent molecules from the nucleophile to the leaving group. In many cases the cluster reaction probably corresponds to eq 2 in which only the reactant ion is solvated.[10] A recent example

$$CH_3X + Y^-(H_2O)_n \rightarrow CH_3Y + X^- + nH_2O \qquad (2)$$

in which solvent-free, monosolvated, and bulk-solvated reactants follow entirely different reaction pathways emphasizes the importance of bulk solvent molecules in determining reaction profiles.[11]

Table I. Calculated Complexation Energies and Intrinsic Barriers (kcal/mol) for $Cl^- + CH_3Cl$

method	complexation energy	intrinsic barrier
3-21G//3-21G	-14.9	5.6
3-21+G//3-21+G	-12.9	5.9
3-21G$^{(*)}$//3-21G$^{(*)}$	-11.4	9.6
6-31G*//6-31G*	-10.3	13.9
exptl	-8.6^a	11.6 ± 1.8^b

^{a}Reference 17. ^{b}Reference 18.

In this paper we report a comprehensive theoretical examination of the reaction between methyl chloride and chloride ion in the gas phase and in aqueous solution using techniques which circumvent the limitations of previous theoretical studies. The calculations involved several steps. First, the gas-phase reaction profile was characterized using high level ab initio calculations by determining the energies and geometries of the $[ClCH_3Cl]^-$ cluster at a number of representative points on the potential surface. The data were then used to develop analytic functions for the calculated geometrical parameters in terms of a well-defined reaction coordinate. The next task was the development of intermolecular potential functions for use in simulating the solution-phase reaction. The TIP4P model was assumed for water monomers[12] and a similar form was also adopted for the solute. However, the parameters in the potential functions for the solute must vary along the reaction. Again, ab initio calculations were employed to obtain a large data base of energies and geometries of solute–water clusters at a variety of points on the potential surface. These results dictated the choice of the functional form as well as the parameters for the solute–water potential function as a function of the reaction coordinate. A second major computational effort then ensued to model the reaction in aqueous solution by using statistical mechanics techniques. A periodic system was employed containing the solute cluster surrounded by 250 water molecules, enough to adequately represent bulk solvent participation in the reaction. The effects of thermal averaging under standard experimental conditions of 25 °C and 1 atm were taken into account through Monte Carlo simulations in the NPT ensemble.[13] Two series of simulations were carried out. In the first set of six Monte Carlo calculations, the importance sampling algorithm of Patey and Valleau was employed in order to obtain the potential of mean force along the reaction coordinate.[14] The resulting free energy curve when compared to the gas-phase ab initio energy profile provides the first direct measure of the influence of solvation on an S_N2 energy profile along the entire reaction coordinate. Consequently, the study also represents the first critical examination of the generally held view that S_N2 reaction profiles are unimodal in solution. We recently communicated the results for the reaction surface from this study,[15] while the full details are provided here. Subsequently, two more Monte Carlo simulations were carried out in which the solute geometry was held fixed at values corresponding to the reactants/products and the transition state. The results of these simulations are also presented in this paper and provide a wealth of structural and energetic data including solute–solvent radial distribution functions, energy distributions, coordination numbers, and hydrogen bonding distributions for the key points on the reaction surface. The overall outcome is an intimate molecular

(6) Review: Dedieu, A.; Veillard, A. In "Quantum Theory of Chemical Reactions"; Daudel, R., Pullman, A., Salem, L., Veillard, A., Eds.; D. Reidel Publishers: New York, 1979; Vol. 1, p 69.

(7) (a) Berthier, G.; David, D.-J.; Veillard, A. *Theoret. Chim. Acta* **1969**, *14*, 329. (b) Dedieu, A.; Veillard, A. *Chem. Phys. Lett.* **1970**, *5*, 328. (c) Dedieu, A.; Veillard, A. *J. Am. Chem. Soc.* **1972**, *94*, 6730. (d) Ritchie, C. D.; Chappell, G. A. *Ibid.* **1970**, *92*, 1819. (e) Duke, A. J.; Bader, R. F. W. *Chem. Phys. Lett.* **1971**, *10*, 631. (f) Bader, R. F. W.; Duke, A. J.; Messer, R. R. *J. Am. Chem. Soc.* **1973**, *95*, 7715. (g) Baybutt, P. *Mol. Phys.* **1975**, *29*, 389. (h) Keil, F.; Ahlrichs, R. *J. Am. Chem. Soc.* **1976**, *98*, 4787. (i) Dyczmons, V.; Kutzelnigg, W. *Theor. Chim. Acta* **1974**, *33*, 239. (j) Cremaschi, O.; Simonetta, M. *Chem. Phys. Lett.* **1976**, *44*, 70. (k) Schlegel, H. B.; Mislow, K.; Bernardi, F.; Bottoni, A. *Theor. Chim. Acta* **1977**, *44*, 245. (l) Wolfe, S.; Mitchell, D. J.; Schlegel, H. B. *J. Am. Chem. Soc.* **1981**, *103*, 7602, 7694. (m) Ishida, K.; Morokuma, K.; Komornicki, A. *J. Chem. Phys.* **1977**, *66*, 2153. (n) Kujimoto, N.; Kosugi, N. *Bull. Chem. Soc. Jpn.* **1977**, *50*, 2209. (o) Talaty, E. R.; Woods, J. J.; Simons, G. *Aust. J. Chem.* **1979**, *32*, 2289. (p) Dewar, M. J. S.; Healy, E. *Organometallics* **1982**, *1*, 1705. (q) Urban, M.; Cernusak, I.; Kello, V. *Chem. Phys. Lett.* **1984**, *105*, 625.

(8) Morokuma, K. *J. Am. Chem. Soc.* **1982**, *104*, 3732. For a related study employing semiempirical methods, see: Cremaschi, P.; Gamba, A.; Simonetta, M. *Theor. Chim. Acta* **1972**, *25*, 237. For a study in which both the nucleophile and the leaving group are solvated by one water molecule, see: Jaume, J.; Lluch, J. M.; Oliva, A.; Bertrán, J. *Chem. Phys. Lett.* **1984**, *106*, 232.

(9) Bohme, D. K.; Mackay, G. I. *J. Am. Chem. Soc.* **1981**, *103*, 978. Bohme, D. K.; Raksit, A. B. *Ibid.* **1984**, *106*, 3447.

(10) Henchman, M.; Paulson, J. F.; Hierl, P. M. *J. Am. Chem. Soc.* **1983**, *105*, 5509.

(11) Caldwell, G.; Rozeboom, M. D.; Kiplinger, J. P.; Bartmess, J. E. *J. Am. Chem. Soc.* **1984**, *106*, 809.

(12) Jorgensen, W. L.; Chandrasekhar, J.; Madura, J. D.; Impey, R. W.; Klein, M. L. *J. Chem. Phys.* **1983**, *79*, 926.

(13) Lykos, P. G., Ed. "Computer Modelling of Matter"; American Chemical Society: Washington, DC, 1978.

(14) Patey, G. N.; Valleau. J. P. *J. Chem. Phys.* **1975**, *63*, 2334. For interesting applications of this technique, see: Pangali, C. S.; Rao, M.; Berne, B. J. *Ibid.* **1979**, *71*, 2975. Northrup, S. H.; Pearl, M. R.; Lee, C.-Y.; McCammon, J. A.; Karplus, M. *Proc. Natl. Acad. Sci. U.S.A.* **1982**, *79*, 4035. Ravishanker, G.; Mezei, M.; Beveridge, D. L. *Faraday Symp.* **1982**, *17*, 79. Berkowitz, M.; Karim, O. A.; McCammon, J. A.; Rossky, P. J. *Chem. Phys. Lett.* **1984**, *105*, 577.

(15) Chandrasekhar, J.; Smith, S. F.; Jorgensen, W. L. *J. Am. Chem. Soc.* **1984**, *106*, 3049.

**Table II.** Geometries and Energies of $ClCH_3Cl^-$ Calculated at the 6-31G* Level[a]

r_{CCl}	$r_{CCl'}$	$-r_c$	r_{CH}	$\angle HCCl'$	$-E$, au	ΔE
∞	1.785	∞	1.078	108.5	958.619 15	0
7.500	1.792	5.708	1.077	108.4	958.622 92	-2.4
6.000	1.795	4.205	1.077	108.3	958.624 89	-3.6
4.500	1.803	2.697	1.076	108.4	958.629 37	-6.4
3.269 (1)	1.828	1.441	1.073	108.0	958.635 50	-10.3
2.974	1.850	1.124	1.071	107.1	958.633 87	-9.2
2.678	1.906	0.772	1.067	104.6	958.626 25	-4.5
2.530	1.992	0.538	1.064	101.2	958.619 06	-0.1
2.383 (2)	2.383	0	1.061	90.0	958.613 47	3.6

[a] Distances in angstroms, angles in degrees, and relative energies in kilocalories per mole.

level description of the structural and energetic changes that occur during the course of an S_N2 reaction in solution.

Gas-Phase Reaction. (a) Ab Initio Calculations. The chloride-exchange reaction in the absence of medium effects was examined by using ab initio molecular orbital theory.[16] A variety of basis sets was tested to determine the theoretical level appropriate for the present problem. At all levels employed, three distinct stationary points on the reaction surface were obtained, viz., the reactants at infinite separation, the unsymmetrical minimum corresponding to an ion–dipole complex, **1**, and the symmetrical transition state, **2**. The latter two structures were obtained by optimizing the $[ClCH_3Cl]^-$ cluster with C_{3v} and D_{3h} symmetry constraints. The relative energies of these points provide excellent calibration for the theoretical models (Table I). Experimentally the complexation enthalpy is known to be -8.6 kcal/mol,[17] while the intrinsic barrier, i.e., the energy of **2** relative to **1**, has been estimated to be 11.6 ± 1.8 kcal/mol.[18] The small 3-21G basis set significantly overestimates the relative stabilities of **1** and **2**. Inclusion of diffuse functions in the basis set, 3-21+G, makes the complexation energy less negative since the bare anion benefits more from the additional basis functions. However, the calculated intrinsic barrier (5.9 kcal/mol) is virtually unchanged. Selective inclusion of d functions on the chlorine atoms in the 3-21G(*) basis set leads to improved prediction for all the relative energies involved, but the agreement with experiment is still not quantitative, particularly for the complexation energy. The extended 6-31G* basis set with d functions on all heavy atoms yields a complexation energy of -10.3 kcal/mol and an intrinsic barrier of 13.9 kcal/mol. The good performance of this theoretical level may be due to fortuitous cancellation of errors arising from incomplete basis sets and neglect of electron correlation. Electron correlation has previously been calculated to contribute as much as +7 kcal/mol to the total activation energy,[7h] although the CEPA method employed appears to have provided an overestimate. A recent study predicts the contribution of electron correlation to have the opposite sign for two model S_N2 reactions.[7q] In any case, the reliable energies calculated at the 6-31G* level for three key points on the potential surface indicate that the level may be able to provide a uniformly good, unbiased description of the reaction profile.

The calculated geometries at the 6-31G* level for the complex, **1**, and the transition state, **2**, are shown in Figure 1. The nature of **1** as an ion–dipole complex is reflected in its geometry. The
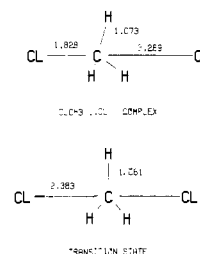
Figure 1. Optimized 6-31G* geometries of **1** and **2**: bond lengths in angstroms, angles in degrees.

CCl bond is stretched slightly to 1.828 Å from the value of 1.785 Å in CH_3Cl, while the other CCl distance is 3.269 Å. The pyramidality of the methyl group in **1** is also close to that in CH_3Cl. At the transition state the two CCl distances are 2.383 Å. The calculated geometric parameters of CH_3Cl and **2** are nearly identical with the values obtained by Keil and Ahlrichs using large basis sets.[7h]

The full reaction profile was constructed by calculating the energies at three points between **1** and **2** (r_{CCl} = 2.530, 2.678, and 2.974 Å) and at three points between **1** and the separated reactants (r_{CCl} = 4.5, 6.0, and 7.5 Å). For each assumed value of r_{CCl}, the remaining geometric parameters were optimized in C_{3v} symmetry. The calculated total and relative energies as well as the optimized geometric parameters are given in Table II. The calculated energy changes are typical of S_N2 reactions in the gas phase.[1,2,6,7] The initial approach of the ion and the polar substrate leads to a smooth reduction in energy until the minimum **1** is formed. Beyond that point the energy increases and reaches a maximum at the symmetrical transition state. However, the calculated geometric parameters exhibit a different behavior. The structural changes are negligible from the separated reactants to the minimum, but large changes take place between **1** and **2**. Interestingly, all the parameters show the qualitative variation.

(b) Analytic Description of the Reaction Surface. Simulation of the solute-phase S_N2 reaction with importance sampling requires a knowledge of the energies and geometries of the solute cluster as a function of the reaction coordinate. Fairly simple analytic functions can be obtained from ab initio data especially since they show no discontinuities. However, the functions are critically dependent on the choice of the reaction coordinate.

The nucleophile, the methyl carbon, and the leaving group are assumed to remain collinear throughout the reaction. A simple choice of the reaction coordinate would then be one of the CCl distances, e.g., r_{CCl} where Cl is the nucleophile. Determination of the minimum energy reaction pathway (MERP) as well as the remaining geometric parameters as a function of r_{CCl} through ab initio geometry optimization is then straightforward. However, there are some advantages in using an alternative definition of the reaction coordinate, r_c, given in eq 3, where Cl' is the leaving group. Unlike r_{CCl} or $r_{CCl'}$, r_c fully reflects the symmetry of the

$$r_c = r_{CCl'} - r_{CCl} \qquad (3)$$

reaction. Thus, in the present case, r_c takes on values of $-\infty$, 0, and ∞ for the reactants, the transition state, and the products, respectively. The corresponding values of r_{CCl} are ∞, 2.383, and 1.785 Å, thus exhibiting a highly uneven variation in the two halves of the reaction. The choice of r_c as the reaction coordinate is

(16) All ab initio calculations were performed on a Harris 80 computer using the GAUSSIAN 82 series of programs: DeFrees, D. J.; Levi, B. A.; Pollack, S. K.; Blurock, N.; Hout, R. F.; Pietro, W. J.; Francl, M. M.; Hehre, W. J. *QCPE*, to be submitted. Geometry optimizations were carried out by using analytically evaluated gradients and multiparameter searches. 3-21G: Binkley, J. S.; Pople, J. A.; Hehre, W. J. *J. Am. Chem. Soc.* **1980**, *102*, 939. Gordon, M. S.; Binkley, J. S.; Pople, J. A.; Pietro, W. J.; Hehre, W. J. *Ibid.* **1982**, *104*, 2797. 3-21+G: Clark, T.; Chandrasekhar, J; Spitznagel, G. W.; Schleyer, P. v. R. *J. Comput. Chem.* **1983**, *4*, 294. 3-21G(*): Pietro, W. J.; Francl, M. M.; Hehre, W. J.; DeFrees, D. J.; Pople, J. A.; Binkley, J. S. *J. Am. Chem. Soc.* **1982**, *104*, 5039. 6-31G*: Hariharan, P. C.; Pople, J. A. *Theor. Chim. Acta* **1973**, *28*, 203. Francl, M. M.; Pietro, W. J.; Hehre, W. J.; Binkley, J. S.; Gordon, M. S.; DeFrees, D. J.; Pople, J. A. *J. Chem. Phys.* **1983**, *77*, 3054.

(17) Dougherty, R. C.; Roberts, J. D. *Org. Mass Spectrom.* **1974**, *8*, 77.

(18) Calculated from the gas-phase data in ref 2b using enthalpy instead of free energy in the Marcus equation: Shaik, S. S.; Pross, A. *J. Am. Chem. Soc.* **1982**, *104*, 2708.
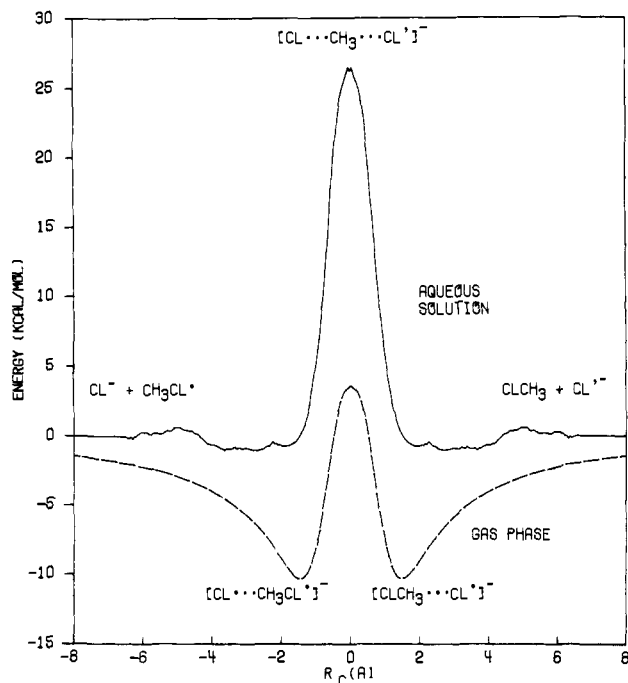
Figure 2. Calculated internal energies in the gas phase (dashed curve) and the potential of the mean force in aqueous solution (solid curve) for the system $[ClCH_3Cl]^-$ as a function of the reaction coordinate, r_c (in angstroms).

especially good for unsymmetrical reactions, which we plan to study in the future. We have chosen to present energy profiles in terms of r_c, although, in the present case, each point on the MERP is characterized by a unique set of r_{CCl}, $r_{CCl'}$, and r_c values. The values are related through eq 3 and 4, the latter being obtained through a least-squares fit of the geometry data in Table II.

$$r_{CCl'} = 0.0918/(r_c^2 + 0.1536) + 1.7850 \qquad (4)$$

The 6-31G* energies in Table II were used to obtain an analytical function for the energy profile in terms of r_c. Least-squares fitting was used to determine the constants in eq 5. A constraint

$$E(r_c) = 192.3/(|r_c| + 1.559)^6 - 140.6/(|r_c| + 1.915)^2 +$$
$$30.45 \exp[-(r_c/0.8682)^2] \quad (5)$$

to make the gradient of the energy vanish at $r_c = 0$ was imposed on the fit. A graphical representation of eq 5 is provided in Figure 2 (dashed curve).

As mentioned in the previous discussion, the geometric parameters $r_{CCl'}$, r_{CH}, and $\angle HCCl'$ show the same qualitative dependence on r_{CCl}. The parameters can all be described by the same functional form, eq 6, with the constants k_1 and k_2 chosen to ensure that the values for the transition state and the reactants are correctly reproduced (Table III). However, the absolute magnitude of the variation of r_{CH} was so small that this parameter

$$f(r_{CCl}) = k_1[0.03167/(r_{CCl} - 1.7567)^6 + 0.22804/r_{CCl}] + k_2 \quad (6)$$

nitude of the variation of r_{CH} was so small that this parameter was held constant at 1.07 Å in the simulations. Also, eq 4 is enough to define $r_{CCl'}$ in terms of r_c for any point on the MERP, making a fit in the form of eq 6 superfluous for this parameter.

Equations 3–6 together with the appropriate values of k_1 and k_2 from Table III provide a complete analytic description of the energies and geometries at all points on the gas-phase MERP and can conveniently be used in the statistical mechanics simulations.

Intermolecular Potential Functions. The solute–solvent and solvent–solvent interactions were assumed to be pairwise additive and were described through Coulomb and Lennard–Jones terms, acting between various sites on the monomers (eq 7). For water,

$$\epsilon_{mn} = \sum_i^{\text{on } m} \sum_j^{\text{on } n} (q_i q_j e^2/r_{ij} + A_i A_j/r_{ij}^{12} - C_i C_j/r_{ij}^6) \qquad (7)$$

Table III. Constants k_1 and k_2 in Equation 6 for the Geometric and Potential Function Parameters[a]

parameter	k_1	k_2
r_{CH}	0	1.07
$\angle HCCl'$	−30.176	108.72
q_H	0.226	0.120
q_C	−0.093	−0.182
$q_{Cl'}$	−0.954	−0.178
q_{Cl}	0.371	−1.000
A_H^2	0	650
A_C^2	0	8.7×10^5
A_{Cl}^2	0	2.6×10^7
$A_{Cl'}^2$	27.4×10^6	9.0×10^6
C_H^2	0	32
C_C^2	0	500
C_{Cl}^2	−1773	2600
$C_{Cl'}^2$	967	900

[a] Distance in Å, angle in degrees. Units for A^2 and C^2 are kcal Å^{12}/mol and kcal Å^6/mol, respectively.

the TIP4P model was chosen,[12] in which the interaction sites are located at the three nuclei and at a fourth point (M) on the bisector of the HOH angle 0.15 Å from the oxygen atom toward the hydrogen atoms. The monomer geometry was held rigid with r_{OH} = 0.9572 Å and $\angle HOH$ = 104.52°. The nonzero charges and Lennard–Jones terms are $2q_H = -q_M = 1.04$, $A_{OO}^2 = 6 \times 10^5$ kcal·Å^{12}/mol and $C_{OO}^2 = 610$ kcal·Å^6/mol. The interaction sites for the solute were located on its atoms. The geometry as well as the q, A, and C parameters of the solute vary along the reaction. The determination of analytic functions for the geometric variations was described in the previous section. We now turn to the problem of deriving similar expressions for the q, A, and C terms for the four distinct sites, Cl, Cl', C, and H, of the solute.

To reduce the complexity of the problem, a simple functional form was chosen for the potential function parameters. Since all the geometric parameters show the same qualitative variation along the reaction, a similar pattern was anticipated for the q, A, and C values. Thus, description of the functional dependency of all the terms by eq 6 was considered. Initial support for this possibility came from the calculated atomic charges obtained from Mulliken population analyses of 6-31G* wave functions which show the same variation as the geometric parameters. However, the functional form was adopted only after a critical test of its adequacy (vide infra).

The specifications of the potential function parameters then reduced to the determination of the constants k_1 and k_2 of eq 6 for the q, A, and C values of the solute atoms. The constants can be uniquely defined if the q, A, and C values are known for the transition state and the reactants. Therefore, the solute parameters at these two points were developed with great care.

A set of parameters for Cl$^-$ was recently determined in this laboratory based on ab initio interaction energies and geometries of Cl$^-$(H$_2$O) and Cl$^-$(HOCH$_3$).[19] The parameters were successfully employed in a simulation of Cl$^-$ in water, yielding structural and thermodynamic data in good agreement with experiment.[19]

The parameters for CH$_3$Cl were chosen to reproduce ab initio results for complexes of CH$_3$Cl with a water molecule. A variety of geometries was considered: hydrogen bonded structures with CClH$_0$ atoms being collinear and bent, a bifurcated structure with both hydrogen atoms of water near the chlorine atom, and geometries in which the oxygen atom approaches the carbon and hydrogen atoms as well as the bisector of the HCH angle in CH$_3$Cl. In each case a local minimum was obtained through constrained geometry optimization at the 3-21G level. 6-31G* energies were then computed for a number of points spanning the 3-21G minimum energy geometries. Thus, several potential energy curves describing the interaction between CH$_3$Cl and water were constructed. The q, A, and C parameters for the atoms in CH$_3$Cl were determined from these data via a nonlinear least-squares

(19) Chandrasekhar, J.; Spellmeyer, D. C.; Jorgensen, W. L. *J. Am. Chem. Soc.* **1984**, *106*, 903.
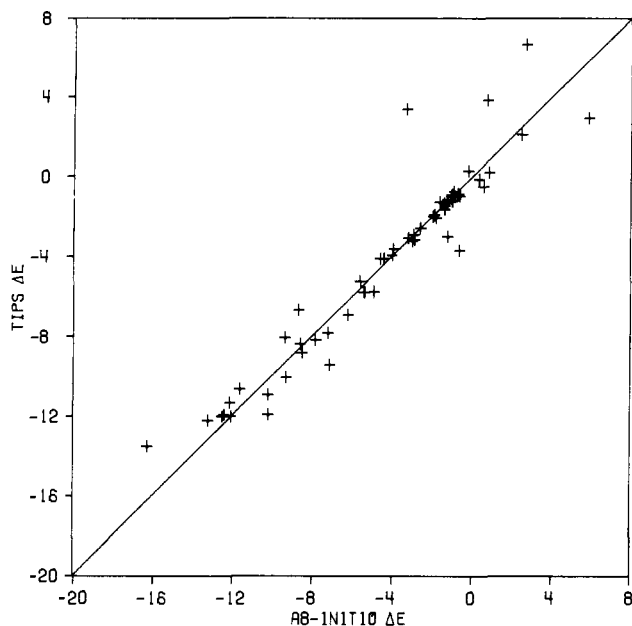
Figure 3. Comparison of the solute–solvent interaction energies predicted by the potential function vs. 6-31G* values. A line of unit slope indicating perfect agreement is shown. All energies in kilocalories per mole.

Figure 4. Predicted geometries of monohydrated clusters of Cl⁻, CH₃Cl, 1, and 2 from the solute–solvent potential functions: bond lengths in angstroms, angles in degrees.

procedure. The corresponding computer program included an efficient geometry optimization routine so that optimum parameters could be obtained which simultaneously gave a good fit to the ab initio interaction energies as well as to the geometries of 6-31G* minima. Thus, the parameters were required to correctly reflect the shapes of the potential energy curves for a variety of approaches of CH_3Cl and water. The final fit was based on 33 interaction energies, 9 geometrical parameters corresponding to local minima, and the dipole moment of CH_3Cl.

A similar approach using 6-31G* energies and geometries of monohydrated structures was employed to obtain the potential function parameters for the transition state. As before, geometries of linear, bent, and bifurcated hydrogen bonded structures as well as those with the water molecule approaching a hydrogen and the bisector of the HCH angle were first optimized at the 3-21G level. Single point 6-31G* calculations around these minima were then performed. A set of q, A, and C parameters was obtained which gave a good fit to the energies and predicted geometries by using the least-squares program mentioned above.

The assumed functional dependency (eq 6) for the potential function parameters was examined next. A large number of 6-31G* calculations was carried out on monohydrated solute clusters at intermediate points along the MERP with $r_{CCl} = 2.974$, 3.269, 4.5, and 6.0 Å. With slight readjustments of the initial set of parameters for the reactants and the transition state, it was possible to obtain generally good agreement between all ab initio and predicted values. The overall performance of the final choice of the potential function can be gauged from Figure 3, which compares the predicted interaction energies of 71 solvated structures with the corresponding 6-31G* values. Although a few discrepancies exist, these are generally confined to repulsive regions on the potential surface. The mean error is only 0.78 kcal/mol for the interaction energies which cover a range of 22 kcal/mol. The simple potential function correctly describes all the key features of the solute–solvent interaction in the system, in particular, hydrogen bonding.

The final choices of k_1 and k_2 for the various parameters are given in Table III. It may be noted that the Lennard–Jones terms for C and H as well as the A parameter for Cl were kept constant over the entire reaction, as they showed negligible variation. Also, the charge on the hydrogen atoms was forced to yield a net unit negative charge for the solute during the simulations.

The optimized structures of the separated reactants, the ion-dipole minimum, and the transition state interacting with a single water molecule each obtained with the solute–solvent potential
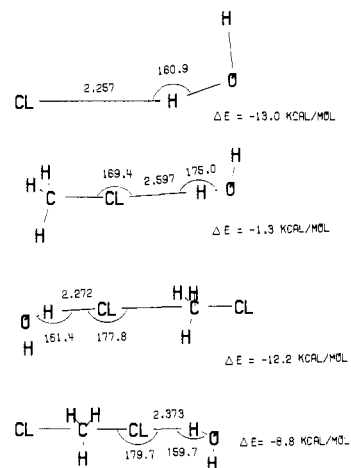
functions are shown in Figure 4. As expected, the interaction energies parallel the charge on the chlorine atom participating in the hydrogen bond. Thus, CH_3Cl forms only a weak hydrogen bond (−1.3 kcal/mol). The predicted interaction energy between Cl⁻ and H_2O (−13.0 kcal/mol) is in excellent agreement with the gas-phase experimental value (−13.1 kcal/mol).[20] The charge on Cl in **1** is not significantly reduced from that in the bare nucleophile, resulting in a monohydration energy of −12.2 kcal/mol. However, the transition state has a more diffuse charge distribution ($q_{Cl} = q_{Cl'} = -0.77$); the solute–water interaction energy is only −8.8 kcal/mol. These values correctly reflect the trend in the solvation energy along the reaction coordinate. However, a full description of solvation requires, in addition to the relative strengths of hydrogen bonds, a knowledge of their number as well as their attenuation with increasing coordination. The role of bulk solvent molecules and thermal averaging needs to be included as well.

Monte Carlo Simulations. The principal goal of this study is the determination of the solution-phase S_N2 reaction profile. While it is straightforward to perform simulations on a few representative points along the reaction, the statistical errors in the calculated differential heats of solution can be of the same order of magnitude as the solvent effect on the activation barrier. A more reliable approach is to determine the solvent-averaged potential of mean force (pmf),$w(r_c)$, which represents the relative free energy of the system as a function of r_c. The function $w(r_c)$ is given by $-k_B T$ ln $g(r_c)$, where $g(r_c)$ is the probability of occurrence of each value of r_c. Precise computation of $g(r_c)$ is not possible through a single long simulation but requires the use of importance sampling.[14] In this procedure, probability distributions are obtained for different overlapping sections of the reaction surface and are combined to obtain a single distribution covering the entire range of r_c. The solute is constrained to remain within limited ranges of r_c by imposing fictitious forces (umbrella potentials). The "windows" are carefully chosen so that all regions of interest on the reaction surface are adequately sampled. The Monte Carlo walk is generated in the usual manner, but the probability of selecting a configuration is made proportional to $e^{-\beta(u+u')}$ rather than to the usual Boltzmann factor $e^{-\beta u}$, where u is the true configurational energy, u' is the biasing umbrella potential added to keep the solute within the chosen window, and $\beta = 1/k_B T$. All calculated properties from such simulations can be normalized to remove the effects of non-Boltzmann sampling.[14] Thus, the true ensemble average of a property Q is given by eq 8, where $\langle \rangle_w$ refers to an average in the biased system. In particular, the

$$\langle Q \rangle = \langle Qe^{\beta u'} \rangle_w / \langle e^{\beta u'} \rangle_w \qquad (8)$$

(20) Arshadi, M.; Yamdagni, R.; Kebarle, P. *J. Phys. Chem.* **1970**, *74*, 1475. Yamdagni, R.; Kebarle, P. *J. Am. Chem. Soc.* **1971**, *93*, 7139.

frequency of occurrence of the solute at a given value of the reaction coordinate in window i, $P_i(r_c)$, leads to the function $g_i(r_c)$ on normalization through eq 8. The distribution $P_i(r_c)$ has to be carefully monitored to ensure that the sampling has thoroughly covered window i. The normalized distributions, $g_i(r_c)$, for adjacent windows are matched at points of maximum overlap of the corresponding $P_i(r_c)$ functions. By splicing the results from all the windows, a single distribution $g(r_c)$ is obtained from which the pmf, $w(r_c)$, is easily calculated.

While the use of importance sampling with heavy biasing of the high-energy regions is essential for the determination of the pmf for the system, the procedure is not well suited for obtaining solute–solvent structure and energy distributions. This is particularly true for windows in which energy changes are large, as in the window containing the transition state. In that window, strong biasing is needed to sample the transition state. Although the resultant sampling is even for the window, the high-energy configurations contribute negligibly to the structure and energy distributions due to the exponential factor in eq 8. The distributions are almost entirely dominated by contributions from low-energy configurations. Therefore, the calculated distributions for the window spanning **2** do not reflect the average solvation of the transition state but only that of the structures near the fringe of the window. To obtain precise information on the nature of solvation for the key points on the reaction surface, viz., the reactants and the transition state, it is necessary to perform simulations in which the solute is frozen at the appropriate geometry. The resultant differential solvation energy is subject to substantial statistical errors, but the radial and energy distributions are quite precise. Both sets of simulations, one with importance sampling over the entire reaction and another on fixed solute structures corresponding to the reactants and the transition state, have been carried out in the present study.

Monte Carlo calculations were performed for the solute cluster and 250 water molecules in the NPT ensemble at 25 °C and 1 atm. The system was placed in a tetragonal box with periodic boundary conditions. The long edge was 1.5 times the remaining edges and averaged 31–32 Å. The ClCCl' unit was constrained to be along the long axis. With these choices, there is sufficient water to adequately solvate the separated reactants without introducing significant edge effects. To enhance solute–solvent statistics, a preferential sampling algorithm was employed.[21] The frequency of attempting a solvent move was made proportional to $1/(r_{CCl}^2 + r_{CCl'}^2 + C)$, where C is a constant chosen to enhance the sampling of the solvent monomers nearest the solute by a factor of 3–4 over distant monomers. Solute moves were attempted every 60th configuration.

Simulations with importance sampling were carried out over six windows, corresponding to different choices of the umbrella potential, u'. As in previous applications, harmonic forces centered at different values of r_c were used in the present study.[14] The force constants were chosen to be progressively smaller when going from the transition-state region to the products region, reflecting the expected steepness of the energy profile. In addition to the harmonic force, it was found necessary to add an exponential biasing potential to ensure uniform sampling, especially near the transition state. The final choice of the umbrella potential is given by

$$u'_i = -25e^{-r_c^2} + 0.5k_i(r_c - r_i)^2 \qquad (9)$$

The values of k_i ($i = 1$–6) are 15.0, 15.0, 10.0, 5.0, 2.5, and 2.0 kcal/mol-Å² and of r_i are 0.0, 0.5, 2.0, 2.8, 4.5, and 5.3 Å.

For each window, equilibration was carried out over 1000–2000 K configurations and the averaging was performed on the next 2600 K configurations. New configurations were selected in the usual Monte Carlo manner. For solvent moves, the chosen monomer was randomly translated in the three Cartesian directions
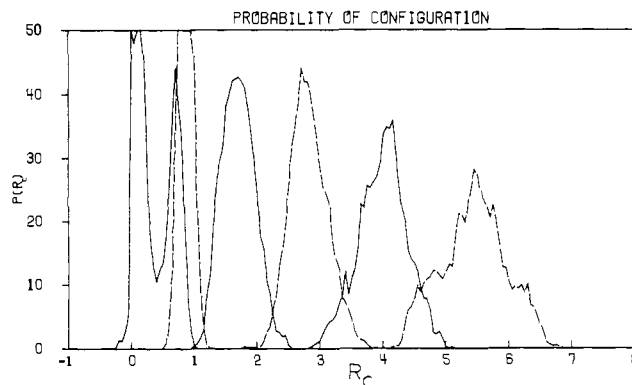
(21) (a) Jorgensen, W. L.; Bigot, B.; Chandrasekhar, J. *J. Am. Chem. Soc.* **1982**, *104*, 4584. (b) Chandrasekhar, J.; Jorgensen, W. L. *J. Chem. Phys.* **1982**, *77*, 5080. (c) Jorgensen, W. L. *Ibid.* **1982**, *77*, 4156. (d) Owicki, J. C. *ACS Symp. Ser.* **1978**, *No. 87*, 159.

Figure 5. Unnormalized probability distribution of solute structures, $P_i(r_c)$, for the six windows obtained from the importance sampling simulations. The abscissa is the reaction coordinate, r_c, in angstroms.

and randomly rotated about a randomly chosen axis. For solute moves, translations were restricted to the long axis and no rotations were performed. The reaction coordinate was randomly changed, and the corresponding new geometry and potential function parameters were evaluated through eq 3, 4, and 6. Volume moves were performed every 2000 configurations by scaling the coordinates.[22] The energy of the new configuration was computed from the pairwise sum over all the interaction energies (eq 7) out to a cutoff radius of 8 Å based on O–O, Cl–O, and Cl'–O distances. The gas-phase solute energy was obtained from eq 5, and the umbrella potential was calculated from eq 9. Acceptance of the new configuration was based on the Metropolis test with the appropriate modifications for the preferential sampling.[21d] The ranges of the moves were chosen to yield an acceptance rate of about 40%. These simulations were performed on the Cyber 205 at Purdue.

Two more simulations were carried out on systems defined as above with the exception that the geometry of the solute was held rigid. In one simulation, the nucleophile was kept 7.5 Å away from the methyl carbon. In the second one, the geometry of **2** was used. In both cases, the appropriate potential function parameters from eq 6 and Table III were employed. The details of the simulations are the same as those described above, including the use of preferential sampling but without the need for umbrella sampling. Initial configurations for these simulations were obtained from equilibrated ones from windows 1 and 6. Additional equilibration was performed for 1000 K configurations, followed by averaging over 2000 K configurations. These calculations were made on a Harris H-80 computer in our laboratory.

Gas-Phase vs. Solution Energy Profiles. The *unnormalized* solute distributions, $P_i(r_c)$, for the six windows are shown in Figure 5. Smooth Gaussian distributions with widths inversely proportional to the harmonic force constants, k_i, would be obtained if the true relative energy of the solution is exactly counterbalanced by the exponential term in the biasing potential (eq 9). This is roughly the case for windows 2–6, whose $P_i(r_c)$ are smooth distributions spanning increasing ranges of r_c. The distribution for the first window has two peaks, indicating that the variation in the pmf in this region is not perfectly compensated by the exponential biasing term. Nevertheless, the region from $r_c = 0$ to 1 Å is adequately sampled in this window. Overall, the distributions for the six windows cover a significant portion of the reaction surface up to $r_c = 7$ Å, which corresponds to a separation of 8.8 Å between the reactants. Also, the distributions for adjacent windows have sufficient overlap to ensure the precision of the splicing process. The values of $g_i(r_c)$ calculated by normalizing $P_i(r_c)$ through eq 8 were matched at points of maximum overlap for $P_i(r_c)$, viz., 0.70, 1.15, 2.25, 3.45, and 4.60 Å, to obtain a single distribution. The potential of the mean force was calculated from the resultant $g(r_c)$ with the zero set at $r_c = 6.6$ Å. The relative free energies have a precision of ±0.5 kcal/mol on the basis of

(22) McDonald, I. R. *Mol. Phys.* **1972**, *23*, 41.

the standard deviations in the calculated $P_i(r_c)$.

Figure 2 compares the solution-phase pmf (solid curve) with the gas-phase energy profile (dashed curve). It is important to note that the former is a free energy curve while the gas-phase profile represents the internal energy change for the hypothetical vibrationless system at 0 K. If zero-point vibrational and thermal corrections are relatively small, the gas-phase enthalpy profile is similar to the ΔE curve. However, it is well-known that the formation of the ion–dipole complex 1 from infinitely separated reactants involves a large negative entropy change. Therefore, the gas-phase well is less deep on the free energy scale. Experimentally, the complexation enthalpy of 1 is −8.6 kcal/mol while the ΔG for the process is only −4.1 kcal/mol.[17] The entropic contribution must be borne in mind while interpreting the initial phase of the profiles in Figure 2. However, the entropy differences in the intrinsic barrier region may be expected to be relatively small since the changes in degrees of freedom are limited. Thus, the calculated gas-phase energy profile (ΔE) may be a good approximation to the free energy curve in this portion of the reaction surface. The most dramatic feature in Figure 2 is the almost unimodal nature of the free energy curve in solution in contrast to the double-well profile in the gas-phase. The symmetric wells with significant depths (ca. 5 kcal/mol on the free-energy scale) are flattened by the effect of solvation. Although small ripples are seen in the solution-phase curve, they are not likely to have any observable effect on the kinetics of the reaction. Thus, the calculated results provide firm support for the traditional view that S_N2 energy profiles are unimodal in aqueous solution.[3]

The second significant result from the simulations is the large increase in activation energy due to solvation. The calculations correctly reproduce the several orders of magnitude rate difference for gas-phase and solution S_N2 reactions. In fact, the calculated free energy of activation (26.3 ± 0.5 kcal/mol) is in quantitative agreement with the experimental value (26.6 kcal/mol).[3d,4,5]

Finally, a detailed consideration of the shape of the solution-phase reaction profile sheds light on the nature of the reaction. The backside approach of Cl⁻ toward methyl chloride leads to the initial formation of the ion–dipole minimum in the gas phase. However, in solution, the ion needs to be desolvated for the ion–dipole complex to form. In the present system, the desolvation is compensated by the ion–dipole attraction. Therefore, there is little net energy change in the solution reaction from the separated reactants up to the formation of 1. The balance is not quite perfect as witnessed by the small energy barrier near $r_c = 5$ Å. The barrier height of 1.6 kcal/mol is substantially larger than the statistical uncertainty in the calculations. However, as mentioned earlier, these features have negligible consequence on the kinetics of the reaction in view of the size of the main barrier.

In contrast to the early part of the reaction, large energy changes occur between 1 and 2. In fact, the entire activation process in solution is basically represented by the transformation of the ion–dipole complex to the symmetric transition state. Part of the barrier (ca. 14 kcal/mol) is due to the intrinsic barrier for the solute, but a significant contribution (ca. 12 kcal/mol) is from the weaker solvation of 2 relative to 1. This result is fully concordant with the rapid delocalization of charge on the chlorine atoms in going from 1 to 2 with a corresponding reduction in solute–water hydrogen bond strengths.

The late onset of the barrier found in the present study has not been anticipated in previous discussions of solution-phase reactions to our knowledge. The initial desolvation of the reactants has generally been considered so important that the activation barrier has been believed to begin, sometimes even be determined, at this stage of the reaction.[3c,e,f] The present calculations show this not to be the case for the aqueous chloride-exchange reaction. The erroneous notion is illustrated in Figure 5.14 of ref 3f and follows from the idea that the desolvation of the nucleophile dominates any nucleophile–substrate attraction.[3e,f] Another point that requires correction appears in the recent MNDO study of gas-phase S_N2 reactions by Carrion and Dewar.[3g] They find the calculated intrinsic barriers for chloride exchange to be the same as their listed, though unreferenced, solution-phase activation enthalpies.
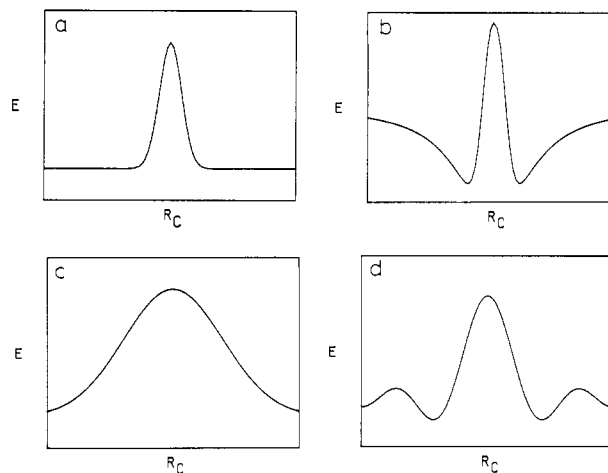
Figure 6. Possible S_N2 reaction profiles in solution when (a) desolvation of nucleophile nearly equals ion–dipole attraction, (b) desolvation is small and/or ion–dipole interaction is strong, (c) desolvation is the only dominant factor, and (d) both desolvation and ion–dipole attraction are significant but are out of phase.

This leads them to conclude that (1) the free energies of solvation of the ion–dipole complex and transition state are similar and, therefore, (2) formation of the complex from the reactants involves little free-energy change in solution. Unfortunately the "experimental" activation enthalpies reported in ref 3g are incorrect and too low.[3d,23] Thus, conclusion (1) above is wrong since there is a substantial solvent induced barrier; however, conclusion (2) fortuitously turns out to be correct for at least Cl⁻ + CH₃Cl in water.

The extent to which the present results, in particular the narrow unimodal shape of the energy profile (Figure 6a), can be generalized to all solution-phase S_N2 reactions is of considerable interest. The key factors determining the overall shape of the energy profile will be present in all systems but in varying magnitudes. It is a safe generalization that a large central barrier will be the dominant feature in all condensed-phase S_N2 reactions. However, a double-well profile as in Figure 6b is possible if the ion–dipole complex exists in a deep minimum in the gas phase and/or if the specific solvation of the nucleophile is relatively weak, making the initial desolvation process facile. This situation could likely be realized in a hydrocarbon solvent, though such a system is not realistic experimentally. It may also be possible in a dipolar aprotic solvent like DMF or Me₂SO. We plan to examine such a system by using the methodology presented here in the near future.[26]

Other interesting variations in the shape of the energy profile are conceivable if the desolvation of the reactants and the onset of ion–dipole attraction are significantly out of phase. If the desolvation is the only dominant energetic factor, a broad unimodal or polymodal reaction profile would result (Figure 6c), as has been suggested previously.[3] However, if the ion–dipole interaction is also large, the energy profile could consist of an initial energy barrier, separating the reactants and the ion–dipole minimum, followed by a central barrier (Figure 6d). Thus, depending on the relative magnitudes of ion–solvent and ion–dipole interactions, a variety of qualitatively different energy profiles are possible for symmetric S_N2 reactions. In general, the nucleophilicity of the ion, dipole moment of the substrate, and steric environment of the nucleophile and electrophile as well as the size, shape, and hydrogen bonding ability of the solvent will all influence the S_N2 reaction profiles.

Some limitations of the present calculations need to be noted. The most serious one concerns the choice of the reaction coordinate. While the linear approach of the nucleophile is a reasonable assumption, alternative pathways covering at least a range of angles around the linear approach must be included for a full

(23) The value was extrapolated from the rate data in: Bathgate, R. H.; Moelwyn-Hughes, E. A. *J. Chem. Soc.* **1959**, 2642.

S_N2 Reaction of Chloride Ion and Methyl Chloride

J. Am. Chem. Soc., Vol. 107, No. 1, 1985 161

Table IV. Results from Simulations on Aqueous Solutions of S_N2 Reactants and the Transition State[a]

	reactants	transition state
E_{sx}	-144 ± 1	-107 ± 1
E_{ss}	-2433 ± 4	-2448 ± 3
E_{ss}^*	-2505 ± 3	-2505 ± 3
ΔE_{ss}	72 ± 5	57 ± 4
ΔE_{sol}	-72 ± 5	-50 ± 4
ΔH_{sol}	-73 ± 5	-51 ± 4
ΔH_{sol} (exptl)	-88^b	
E_{xx}	-2.4	3.6
E_{tot}	-2579 ± 4	-2551 ± 4
ΔE_{tot}	0	28 ± 6
ΔE_{tot} (exptl)	0	23 ± 3^c
V	7840 ± 22	7685 ± 17
V^*	7610 ± 16	7610 ± 16
ΔV_{sol}	230 ± 27	75 ± 23
coordination no.		
Cl	7.0	3.9
Cl'	$17-18$	4.1

[a] All computed values are for one solute and 250 water monomers. Values for the pure solvent are indicated by an asterisk and are calculated from data in ref 12. [b] Reference 24. [c] Reference 23.

description of the reaction surface. Unfortunately, extensions beyond a single dimension are beyond the scope of simulation methods with current resources. Other improvements to the present calculations which entail significant computational effort are the inclusion of explicit three-body interactions and vibrational effects.

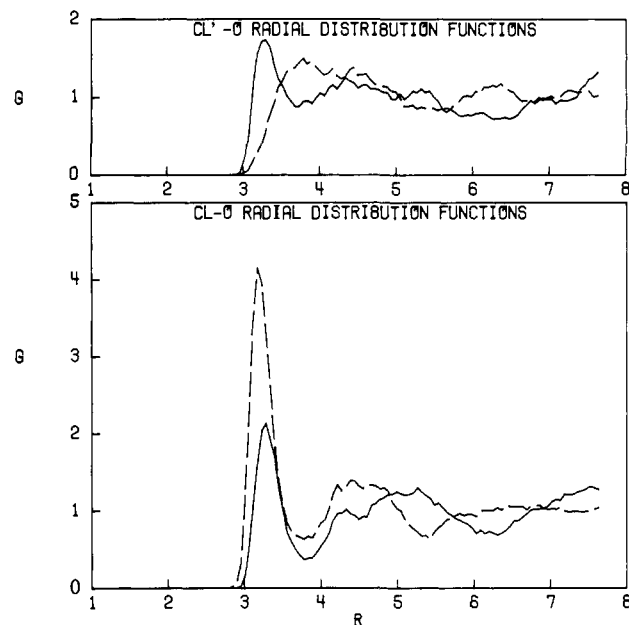**Differential Solvation of the Reactants and the Transition State. (a) Thermodynamics.** The results obtained from the simulations with fixed geometries of the separated reactants and the transition state provide a direct measure of the differential solvation effect on the reaction. The calculated energetic results for the two solute structures are given in Table IV. The energy of solution is defined by eq 10, where E_{sx} is the solute–solvent energy, E_{ss} is the solvent–solvent interaction energy, E^*_{ss} is the energy of the pure solvent (obtained from an earlier study of TIP4P water),[12] and ΔE_{ss} is the solvent reorganization energy. The enthalpy of solution

$$\Delta E_{sol} = E_{sx} + E_{ss} - E^*_{ss} = E_{sx} + \Delta E_{ss} \qquad (10)$$

is then $\Delta H_{sol} = \Delta E_{sol} + P\Delta V_{sol} - RT$, where ΔV_{sol} is the volume of solution and the RT term represents the PV contribution of the solute in the ideal gas. Finally, the solution activation energy is the difference between the two energies of solution plus the change in the energy of the solute (E_{xx}) at the assumed geometries. The values of E_{xx} were obtained from the gas-phase potential, eq 5. Table IV also includes error bars ($\pm\sigma$) estimated from separate averages over blocks of 50 K configurations.

The reactants are significantly better solvated than the transition state; the heats of hydration differ by 22 kcal/mol. Inclusion of solute energies leads to an activation barrier of 28 ± 6 kcal/mol for the reaction. This value is subject to large error bars compared to the activation free energy obtained above with the importance sampling. Nevertheless, the results are consistent, and the calculated activation energy is in good agreement with the enthalpy of activation (23 ± 3 kcal/mol) estimated from nondegenerate halide-exchange reaction rates in water.[23] An additional test for the accuracy of the calculations is provided by the predicted heat of solution of the reactants (-73 ± 5 kcal/mol), which is close to the experimental value of -88 ± 10 kcal/mol.[24]

The major contribution to the calculated barrier is from the change in solute–solvent energy. The E_{sx} term for **2** is 37 kcal/mol less exothermic than for the reactants. But the strong solute–solvent interaction in the solution of the reactants is accompanied by greater disruption of the solvent. Thus, the ΔE_{ss} term is 15

(24) Experimental enthalpies of hydration for CH₃Cl and Cl⁻ are -5.6 and -82 kcal/mol, respectively: Alexander, D. M.; Hill, D. J. T.; White, L. R. *Aust. J. Chem.* **1971**, *24*, 1143. Abraham, M. H. *J. Chem. Soc., Perkin Trans 2* **1973**, 1839. Bockris, J. O'M.; Reddy, A. K. N. "Modern Electrochemistry"; Plenum Press: New York, 1970; Vol. 1, p 106.

Figure 7. Computed Cl–O and Cl'–O rdf's for the solution of the reactants (dashed curve) and the transition state (solid curve). Distances are in angstroms throughout.
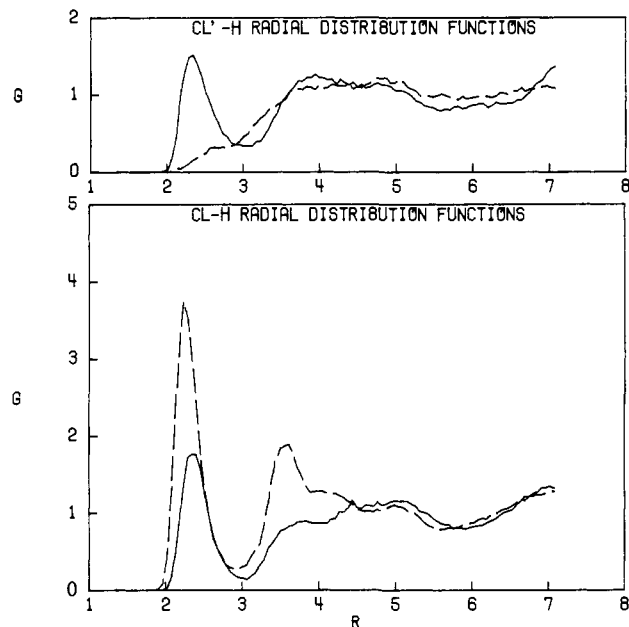
Figure 8. Computed Cl–H and Cl'–H rdf's for the solution of the reactants (dashed curve) and the transition state (solid curve).
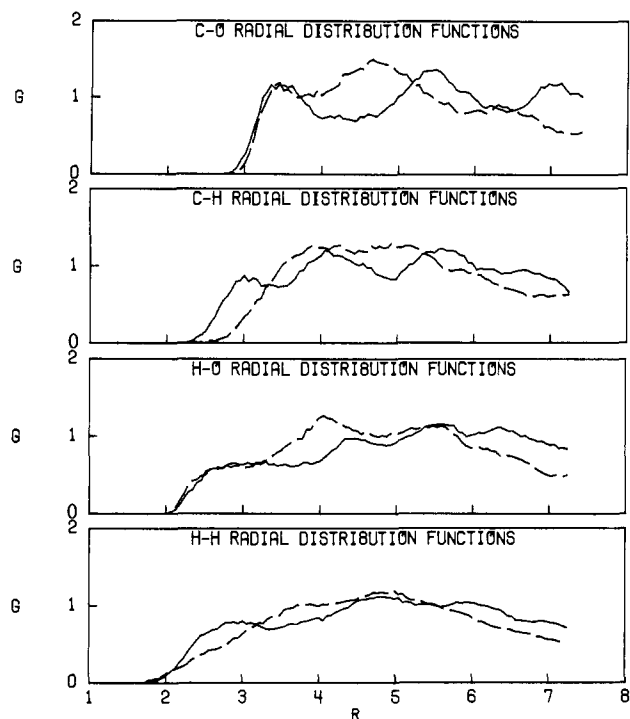
kcal/mol more repulsive in this case. Such an opposing trend in the contribution of solute–solvent and solvent reorganization terms to the total heat of solution is a common feature in solutions of ions in highly structured solvents like water.[19,21a–c]

The volumes of solution obtained from the present NPT simulations (Table IV) are subject to substantial statistical errors. Apart from the fact that some expansion accompanies the introduction of the solutes in water, the values have little interpretive value. However, it is apparent that no gross errors have occurred and the density of the water remains near the TIP4P and experimental value of 1.00 g cm⁻³ at 25 °C and 1 atm.[12]

(b) Solute–Solvent Structure. The structural manifestation of differential hydration may be reflected in solute–solvent radial distribution functions (rdf's). The two chlorine–oxygen distributions g_{ClO} and $g_{Cl'O}$ (Cl is the nucleophile) are shown in Figure 7. The corresponding chlorine–hydrogen distributions are compared in Figure 8. The remaining solute–water distributions, g_{CO}, g_{CH}, g_{HO}, and g_{HH}, are presented in Figure 9 where the first

Figure 9. Computed C–O, C–H, H–O, and H–H rdf's for the solutions of the reactants (dashed curve) and the transition state (solid curve).

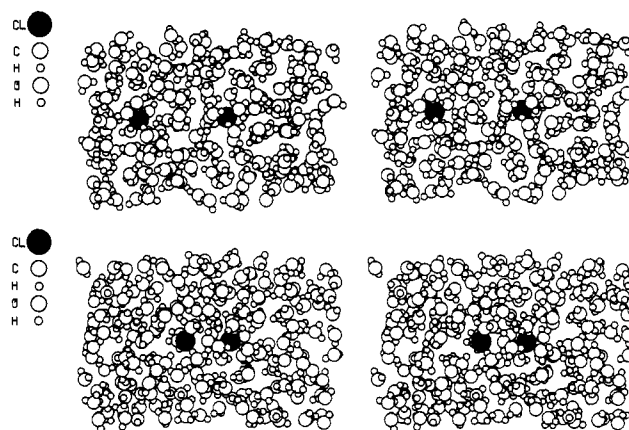**Figure 10.** Stereoplots from a configuration in the simulations of (top) the reactants in water, and (bottom) the transition state in water. A 5.5 Å thick layer of water monomers has been removed in each case to improve clarity.

subscript always refers to the solute atom. In these figures, the solid and dashed curves correspond to the solution of the transition state and reactants, respectively. Although Cl and Cl' are equivalent for the transition state, rdf's for the two atoms were independently evaluated to gauge the convergence of the distributions.

The Cl–O distribution for the transition state has a sharp first peak centered at 3.3 Å, corresponding to the shell of water molecules hydrogen bonded to the chlorine. The second peak is broad, covering a range of over 2 Å. The splitting observed in this peak may result from contributions from both the first shell of water molecules around the methyl group and the second shell for the chlorine. The rise near 8 Å can be attributed to the first shell of water molecules around the chlorine at the opposite end of the solute. In general, radial distribution functions with such long range fluctuations are to be expected for large solutes with widely separated solvent orienting groups.

The two peaks in $g_{Cl'O}$ are broad for the solution of the reactants, since the chlorine atom belongs to the neutral substrate. On the other hand, the corresponding g_{ClO} distribution exhibits a sharp first peak as well as a well-defined second peak. This distribution is very similar to the one obtained in an earlier simulation of Cl⁻ in water.[19] Compared to g_{ClO} for the transition state, the first peak height is significantly higher but the positions are similar.

The above pattern is observed in the calculated Cl–H distributions as well. The first two peaks for the free nucleophile occur at only slightly shorter distances than those for the transition state, but the heights are nearly twice as high, reflecting the relative ability of the solutes to form hydrogen bonds to the solvent. The corresponding feature in $g_{Cl'H}$ for methyl chloride is present only as a shoulder near 2.8 Å of a single, broad peak. The long range variations in all the chlorine–hydrogen distributions are similar. This may be fortuitous since the rise near 7 Å for the transition state is due to water molecules directly hydrogen bonded to the other chlorine atom in the solute.

As alluded to above, g_{ClO} and $g_{Cl'O}$ as well as g_{ClH} and $g_{Cl'H}$ for the transition state should be the same since Cl' and Cl are identical in this case. The agreement is not quantitative in Figures 7 and 8, though the differences are not severe. Solute–solvent rdf's converge slowly even with preferential sampling in comparison to solvent–solvent distributions due to the low solute concentration. There appears to be a small memory effect in the present simu-

lation for the transition state since the distributions for the chlorine that was the nucleophile are somewhat more structured.

The rdf's involving the methyl group differ substantially for the reactants and the transition state, although the potential function parameters for C and H vary only modestly. Of course, the solute geometries differ substantially with the carbon in **2**, being shielded in all directions. The hydrogen bonding to the chlorines also strongly influences all the rdf's.

For both methyl chloride and **2**, the position and height of the first peak in g_{CO} are similar. This is true for g_{HO} as well, indicating that the nearest contacts between oxygen atoms and the methyl group are similar in the two systems. However, the first peaks in g_{CH} and g_{HH} are significantly drawn in for the transition state. This is clearly due to the orienting influence of the negatively charged chlorine atoms close to the methyl group in **2**. The uneven variation of water density around the transition state is reflected in multiple long-range peaks in the g_{CO}, g_{CH}, g_{HO}, and g_{HH} distributions. Most of the peak positions can be matched with maxima observed in distributions involving chlorine atoms after allowing for C–Cl and C–H distances in the solute. For example, the peaks near 5.5 and 7 Å in g_{CO} reflect the first and second shells of water around the chlorines. Even for the reactants, part of the oxygen shell 3.2 Å from the nucleophile coincides with the peak near 4.5 Å in the g_{CO} distribution. The peak near 4 Å in g_{HO} of the reactants has similar contributions.

In summary, the solute–solvent rdf's show structural organization around the solutes for both the reactants and the transition state. The orienting influence of the chlorine atoms leads to well-defined features in the distributions involving other solute atoms as well. Each of the two chlorine atoms of **2** is surrounded by two shells of water molecules, of which the first shell participates in solute–solvent hydrogen bonding. For the reactants, the nucleophile has two well-defined solvation shells. The solvation of methyl chloride is weak with little distinct structure, which is typical for the hydration of mildly polar substrates.

By integrating the rdf's to the minimum after the first peak, coordination numbers can also be obtained. Each of the chlorine atoms in **2** is found to be coordinated to 4.0 ± 0.1 water molecules. In comparison, the coordination number calculated for the nucleophile is 7.0, which is close to the value of 7.4 obtained for the bare ion in an earlier simulation.[19] The broad $g_{Cl'O}$ first peak for methyl chloride integrates to a value of 17–18. While the large coordination number of CH_3Cl contributes little to the solute–solvent energy, the difference in the solvation of Cl⁻ and **2** is the principal cause of the differential solvation energy. The present calculations do not support the contention that the transition state with a diffuse charge distribution forms fewer hydrogen bonds than the nucleophile. The differential solvation effect is caused by the decreased *strength* (Figure 4 and vide infra) rather than *number* of hydrogen bonds for the transition state as compared to the reactants.
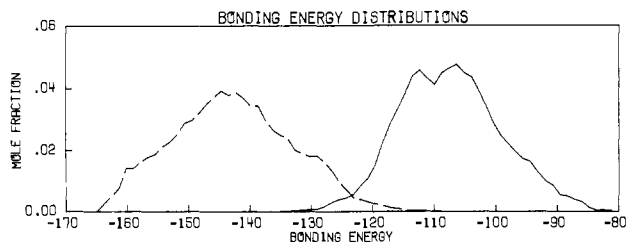
Figure 11. Computed solute–solvent bonding energy distributions for the reactants (dashed curve) and the transition state (solid curve) in water. The ordinate gives the mole fraction of solute with the bonding energy shown on the abscissa. Units for the ordinate are mole fraction per kilocalories/mole.
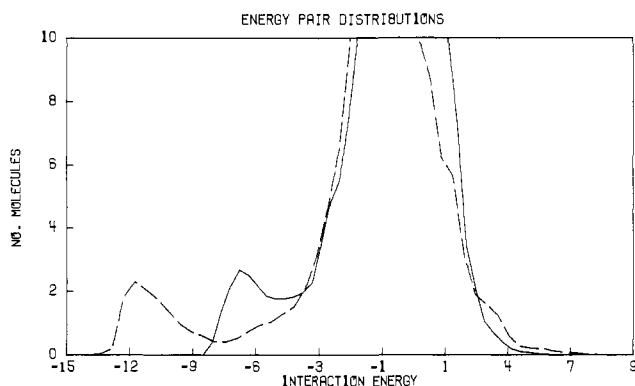
Figure 12. Computed solute–solvent energy pair distributions for the reactants (dashed curve) and the transition state (solid curve) in water. The ordinate records the number of solvent molecules bound by the solute with the energy given on the abscissa. Units for the ordinate are molecules per kilocalories/mole.

The structural notions derived from the solute–solvent rdf's are reinforced by stereoplots of typical configurations obtained from the two simulations (Figure 10). A 5.5 Å thick layer of water monomers has been removed from the front to improve clarity. The hydrogen bonds formed to the two chlorines in **2** as well as to the nucleophile are clearly seen. The arrangement of the remaining water molecules appears to be determined by the need to establish the hydrogen bonding network of the solvent. This is because the solute–solvent interactions become rapidly weaker than solvent–solvent interactions beyond the first shell.[19]

(c) **Energy Distributions.** The calculated solute–solvent bonding energy distributions for the separated reactants and the transition state are compared in Figure 11. While both distributions are broad, covering a range of 50 kcal/mol, the reactants have significantly more attractive bonding energies. This is a consequence of the stronger hydrogen bonds formed by the nucleophile as shown by the calculated solute–solvent energy pair distributions (Figure 12). As in all such distributions, the bulk of the water monomers are at large distance and have very weak interactions with the solute, resulting in the main peak centered near 0 kcal/mol. However, for both the reactants and the transition state, a significant number of highly attractive interactions are present as reflected in the low-energy peak in the distributions. Integration of the peak yields 6.3 and 6.6 as the number of water monomers strongly hydrogen bonded to the reactants and transition state, respectively. While these numbers are similar, the most attractive interaction (−14.0 vs. −8.5 kcal/mol) was well as the average hydrogen bond strength (−11.8 vs. −7.0 kcal/mol) are larger in

magnitude for the reactants. The difference in the solute–solvent energies for the first shell obtained from these distributions almost entirely accounts for the total difference in the E_{sx} term for the two simulations. Minor corrections are produced by the presence of water monomers with significant repulsion toward the solute in the case of the reactants. The existence of monomers which defy solute repulsion in order to smoothly link the first shell monomers to the bulk through solvent–solvent hydrogen bonding has been noted in earlier simulations of ions in water.[19,21b,c]

We have also calculated solvent–solvent rdf's and energy distributions for the two simulations. The results are virtually identical with each other and to those obtained for pure water.[12] This is not surprising since these properties are completely dominated by contributions from bulk solvent molecules which remain unchanged in dilute solutions.

Conclusions. A comprehensive examination of the S$_N$2 reaction between Cl$^-$ and CH$_3$Cl in the gas phase and aqueous solution has been carried out through the use of quantum and statistical mechanics methods. The gas-phase reaction features two equivalent ion–dipole minima separated by a symmetric transition state. In aqueous solution, the ion–dipole attraction is nullified by the energy required to partially desolvate the ion. Also, the transition state with a dispersed charge distribution forms weaker hydrogen bonds to the solvent. Consequently, a nearly unimodal energy profile with a large, narrow, central barrier is calculated for the reaction in aqueous solution. The calculated complexation energy and intrinsic barrier for the gas-phase reaction as well as the heat of hydration of the reactants and the free energy of activation in solution are in excellent agreement with experiment. The form of the reaction surface in water has also been reproduced recently through extended RISM calculations.[25]

Both the nucleophile and the transition state form well-defined solvation shells with nearly the same coordination number, while the neutral substrate is only weakly solvated. The solvation of the reactants is accompanied by a greater solvent disruption energy. The principal contribution to the differential solvation effect comes from the greater strength of the hydrogen bonds formed by the nucleophile.

The present calculations illustrate the power of current theoretical methods in providing both qualitative and quantitative information regarding complex chemical processes even in a condensed phase. The study also represents the rapid widening of scope of statistical mechanics simulations. Within a short period of time, applications have moved along the series: pure solvents, dilute solutions, simple processes in solution like conformational changes, and now to a complex chemical reaction of fundamental importance in organic chemistry. Future studies of reaction surfaces and reaction dynamics for a variety of organic processes may be anticipated.

(25) Chiles, R. A.; Rossky, P. J. *J. Am. Chem. Soc.* **1984**, *106*, 6867.
(26) **Note Added in Proof:** The reaction has now been simulated in liquid DMF at 25 °C (Chandrasekhar, J.; Jorgensen, W. L., submitted for publication). The reaction profile is found to be intermediate between those for the reaction in the gas phase and in aqueous solution. The ion–dipole complexes which are free energy minima in the gas phase are still minima in DMF. Thus, the reaction in DMF involves initial formation of the complex before the rate-determining step. This necessitates revision of the traditional notion that S$_N$2 reactions in solution are concerted processes without intermediates.